Lithos 212–215 (2015) 266–279

Contents lists available at ScienceDirect

Lithos

journal homepage: www.elsevier.com/locate/lithos

Petrogenesis and tectonic implications of Late Carboniferous A-type granites and gabbronorites in NW Iran: Geochronological and geochemical constraints

Hadi Shafaii Moghadam [a,b,*], Xian-Hua Li [a], Xiao-Xiao Ling [a], Robert J. Stern [c], Jose F. Santos [d], Guido Meinhold [e], Ghasem Ghorbani [b], Shirin Shahabi [b]

[a] State Key Laboratory of Lithospheric Evolution,, Institute of Geology and Geophysics, Chinese Academy of Sciences, Beijing 100029, China
[b] School of Earth Sciences, Damghan University, Damghan 36716-41167, Iran
[c] Geosciences Dept., University of TX at Dallas, Richardson, TX 75083-0688, USA
[d] Geobiotec, Departamento de Geociências, Universidade de Aveiro, 3810-193 Aveiro, Portugal
[e] Geowissenschaftliches Zentrum der Universität Göttingen, Goldschmidtstraße 3, D-37077 Göttingen, Germany

ARTICLE INFO

Article history:
Received 17 September 2014
Accepted 11 November 2014
Available online 15 November 2014

Keywords:
A-type granite
Gabbronorite
Carboniferous
Zircon U–Pb ages
Iran

ABSTRACT

Carboniferous igneous rocks constitute volumetrically minor components of Iranian crust but preserve important information about the magmatic and tectonic history of SW Asia. Ghushchi granites and gabbronorites in NW Iran comprise a bimodal magmatic suite that intruded Ediacaran–Cambrian gneiss and are good representatives of carboniferous igneous activity. Precise SIMS U–Pb zircon ages indicate that the gabbronorites and granites were emplaced synchronously at ~320 Ma. Ghushchi granites show A-type magmatic affinities, with typical enrichments in alkalis, Ga, Zr, Nb and Y, depletion in Sr and P and fractionated REE patterns showing strong negative Eu anomalies. The gabbronorites are enriched in LREEs, Nb, Ta and other incompatible trace elements, and are similar in geochemistry to OIB-type rocks. Granites and gabbronorites have similar $\varepsilon_{Nd}(t)$ (+1.3 to +3.4 and −0.1 to +4.4, respectively) and zircon $\varepsilon_{Hf}(t)$ (+1.7 to +6.2 and +0.94 to +6.5, respectively). The similar variation in bulk rock $\varepsilon_{Nd}(t)$ and zircon $\varepsilon_{Hf}(t)$ values and radiometric ages for the granites and gabbronorites indicate a genetic relationship between mafic and felsic magmas, either a crystal fractionation or silicate liquid immiscibility process; further work is needed to resolve petrogenetic details. The compositional characteristics of the bimodal Ghushchi complex are most consistent with magmatic activity in an extensional tectonic environment. This extension may have occurred during rifting of Cadomian fragments away from northern Gondwana during early phases of Neotethys opening.

© 2014 Elsevier B.V. All rights reserved.

1. Introduction

A-type granites are generated in post-collisional and anorogenic settings associated with alkaline-type mafic rocks (Bonin, 2007; El Dabe, 2013). These occur mostly as bimodal magmatic suites accompanying post-collisional extension and/or anorogenic rifting (Bonin, 2004; Eby, 1992). Eby (1990) subdivided A-type granites into two groups according to their tectonic setting and chemistry; 1 — A_1 granites are fractional crystallization products of OIB-like mafic melts associated with intraplate settings or continental rifts; 2 — A_2 granites are partial melting products of juvenile continental crust and are commonly associated with post-collisional extension.

Large volumes of igneous rocks were emplaced as a result of Late Paleozoic subduction beneath Eurasia, which was followed by post-collisional high-temperature–low pressure (HT–LP) metamorphism and magmatism (Stampfli and Borel, 2002; von Raumer et al., 2009). Granites – especially A-type granites – are an important manifestation of this Late Paleozoic 'Hercynian' magmatism. Late Paleozoic alkaline rocks and A-type granites occur in the Eastern Pontides–Lesser Caucasus and NW Iran and give important clues on the geodynamic evolution of these regions during Carboniferous–Permian time (Fig. 1) (e.g., Okay et al., 2001; Topuz et al., 2010; Topuz et al., 2007; Rolland et al., 2011; Rolland et al., 2009). Late Paleozoic magmatism in Turkey is distributed mainly in Sakarya and in the Eastern Pontides (Dokuz et al., 2011; Meinhold et al., 2008; Okay et al., 1999, 2008). The Eastern Pontides contain numerous Hercynian domains, characterized by HT–LP metamorphic rocks (Dokuz et al., 2011; Topuz et al., 2010).

The Iran–Anatolia region is a tectonically active plateau between the converging Arabian and Eurasian plates, which grew as a result of the northward subduction of the Neotethys Ocean beginning in Late Cretaceous time followed by collision between the two plates beginning in Miocene time (Berberian and King, 1981; Chiu et al., 2013; Moghadam

* Corresponding author at: Institute of Geology and Geophysics, Chinese Academy of Sciences, Beijing 100029, China. Tel.: +86 10 82998443; fax: +86 10 62010846.
E-mail address: hadishafaii@mail.iggcas.ac.cn (H.S. Moghadam).

http://dx.doi.org/10.1016/j.lithos.2014.11.009
0024-4937/© 2014 Elsevier B.V. All rights reserved.

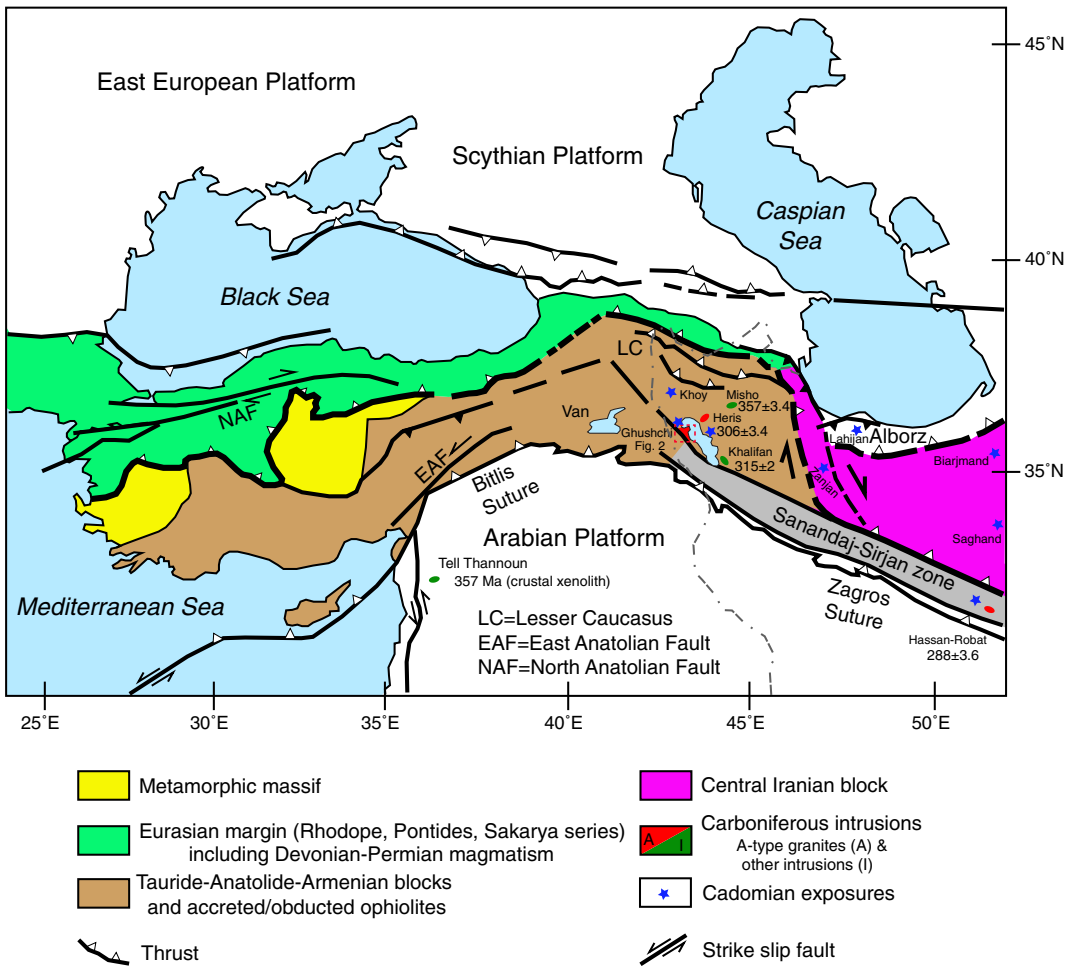

Fig. 1. Sketch geological map of the Caucasus–Turkey and NW Iran regions with emphasis on the distribution of Hercynian magmatism (modified after Rolland et al., 2011).

et al., 2014a). Because of abundant younger rocks (mostly due to Cenozoic volcanism and sedimentation) in Iran, Late Paleozoic igneous rocks are rarely exposed except rare plutons in NW Iran such as Khalifan, Hassan-Robat and Heris granitoids and the mafic Misho intrusion (Fig. 1) (Advay and Ghalamghash, 2011; Alirezaei and Hassanzadeh, 2012; Bea et al., 2011; Saccani et al., 2013) (Fig. 1).

In this paper we present the first detailed petrologic and geochronologic study of an excellent representative of Late Paleozoic igneous activity in the region: the Ghushchi intrusive complex of NW Iran. Our studies include: 1) a detailed investigation of A-type granite and associated OIB-like gabbronorite in terms of mineral and whole rock geochemistry; 2) U–Pb zircon dating of intrusive rocks and their host basement rocks; and 3) bulk rock Sr–Nd and zircon Hf isotope geochemistry. Based on these results, we evaluate the petrogenesis of Late Carboniferous Ghushchi complex A-type granites and OIB-gabbronorites and explore the tectonic implications of this intrusion.

2. Geological setting

2.1. Regional geology

NW Iran and adjoining areas, including NE Turkey and Lesser Caucasus, is a complex zone with a core of Late Neoproterozoic–Early Cambrian crust (ca. 500–600 Ma). These "Cadomian" fragments are stitched together by Paleozoic and Mesozoic sutures and covered by huge expanses of Cenozoic volcanic rocks (Shafaii Moghadam and Stern, 2014).

Northern Iran–southern Eurasia is remarkable for the presence of Paleozoic sutures and associated subduction-related magmatic rocks. In southern Eurasia, the Paleotethys Ocean opened in Early Paleozoic time and closed during Triassic time, resulting in Eo-Cimmerian deformation in northern Iran and Afghanistan followed by Middle–Late Jurassic compression (Boulin, 1991; Zanchetta et al., 2013; Zanchi et al., 2006). Paleotethys opening is reflected in widely distributed alkali to tholeiitic continental flood basalts (Soltan–Meidan basalts), felsic–mafic plutons (with ages of ca. 460 Ma; Shafaii Moghadam and Stern, 2014) and dolomites, evaporites and terrigenous sediments in the Ordovician Ghelli to Lower Devonian Padeha Formations of northern Iran (Aharipour et al., 2010; Stampfli et al., 2001). New zircon U–Pb dating of Masshad 'ophiolite' in NE Iran also reveals evidence of Paleotethys subduction during Devonian time; ca. 380–382 Ma (Moghadam et al., 2014b).

The study area in NW Iran consists of Cadomian basement, Paleozoic platform sediments, and Paleozoic to Triassic igneous rocks, like the geologic succession of central Iran (Alavi, 1991; Berberian and King, 1981). The Late Neoproterozoic Kahar Formation consisting of metasediments and meta-igneous (felsic) rocks is common in NW Iran, Central Iran, as well as in the Alborz and Sanandaj–Sirjan Zones, and is overlain by Cambrian–Ordovician sedimentary rocks including (from bottom to top) (Berberian and King, 1981): (1) Cambrian Soltanieh dolomites with sandstone intercalations; (2) Cambrian Barut sandstones; (3) Ordovician Zagun–Lalun sandstones and quartzites; and (4) Ordovician Mila sandy limestones with shales and marls.

Ediacaran–Cambrian (Cadomian) metamorphosed igneous rocks (orthogneisses) and meta-sediments are also present in NW Iran. The trace of Early Carboniferous rifting to open Neotethys is also recorded

in the Misho Magmatic complex (NW Iran) where gabbros and dikes intrude Cadomian basement (Saccani et al., 2013). Misho gabbros yield a U–Pb zircon age of 356.7 ± 3.4 Ma (Saccani et al., 2013).

2.2. Field occurrence

Ghushchi complex gabbronorite and granite each define belts of discontinuous outcrops ~20 km long WNW–ESE and ~6 km wide NNE–SSW (Fig. 2). The Ghushchi complex intrudes Cadomian basement and is unconformably overlain by Permian–Triassic sediments in the southwest and by Urumieh Lake deposits in the NE (Fig. 2). The composite pluton has been tilted westward, as shown by overlying Permian limestones. The now-vertical gabbronorite–granite contact may once have been horizontal, certainly it dipped less originally. Granitic rocks are subdivided into perthitic alkali-feldspar (AF) granites and amphibole-biotite syeno-granites (and rare AF-quartz syenites). A transition zone characterized by amphibole-biotite syeno-granites occur between the granites and the gabbronorites, whereas perthitic AF-granites dominate away from the gabbronorites. Granites are intruded by thin (0.5 m) to thick (>5–6 m) aplitic dikes. Diabasic dikes and orthoclase-amphibole-rich dikes are also common. Granitic apophyses crosscut the gneisses, and the granite contains Cadomian gneissic xenoliths. Granites and gabbronorites were emplaced about the same time, as demonstrated by injection of granitic dikes into the gabbronorite (Fig. 3a,b) and presence of granitic stocks intruding the gabbronorite (Fig. 3c, d). There are also irregular granitic dikelets within the gabbronorite (Fig. 3e). Evidence of magma mingling is observed near the gabbronorite–granite contact, which is often marked by concentrations of amphibole, biotite–phlogopite, tourmaline and epidote. Gabbronorites are fresh in outcrop and crosscut by 50–100 meter thick diabasic dikes. Gabbronorites are usually fine to medium-grained and sometimes are porphyritic. Gabbronorite is massive and isotropic in the field and no igneous layering is observed. Gabbronorites are mostly homogenous but in some places they show feldspar accumulation.

Locations of samples investigated in this study are shown in Fig. 2. Most samples are from eastern parts of the intrusion as the western parts are highly altered. The Ghushchi complex intruded Late Neoproterozoic–Paleozoic (Cadomian) metamorphic rocks including granitic gneisses, amphibolites and meta-sediments. Gneissic rocks contain large (2–3 cm) alkali feldspar phenocrysts with abundant biotite and are foliated. Amphibole is another rock-forming mineral that usually shows elongation.

3. Petrography and mineral geochemistry

In this section we describe petrography and mineral geochemistry of the Ghushchi gabbronorites and granites. Analytical methods for whole rock major, trace, REE, mineral composition and bulk rock Sr–Nd and zircon Hf isotopic analyses as well as U–Pb zircon dating are presented in Supplementary Document 1.

3.1. Gabbronorites

Gabbronorites are fine- to medium-grained and melanocratic. Intergranular, sub-ophitic and poikilitic textures are common. These rocks contain euhedral to subhedral plagioclase laths (av. 1–2 mm) (50–60% vol.), clinopyroxene (20–30%) and orthopyroxene (10–15%) (Fig. 4a and b). Large plagioclase phenocrysts have orthopyroxene inclusions. These three are early-formed phases while biotite and amphibole are late phases. Biotite (3–5%) is the other important rock-forming mineral whereas amphibole (2–3%), iron oxides (titano-magnetite) (1–2%),

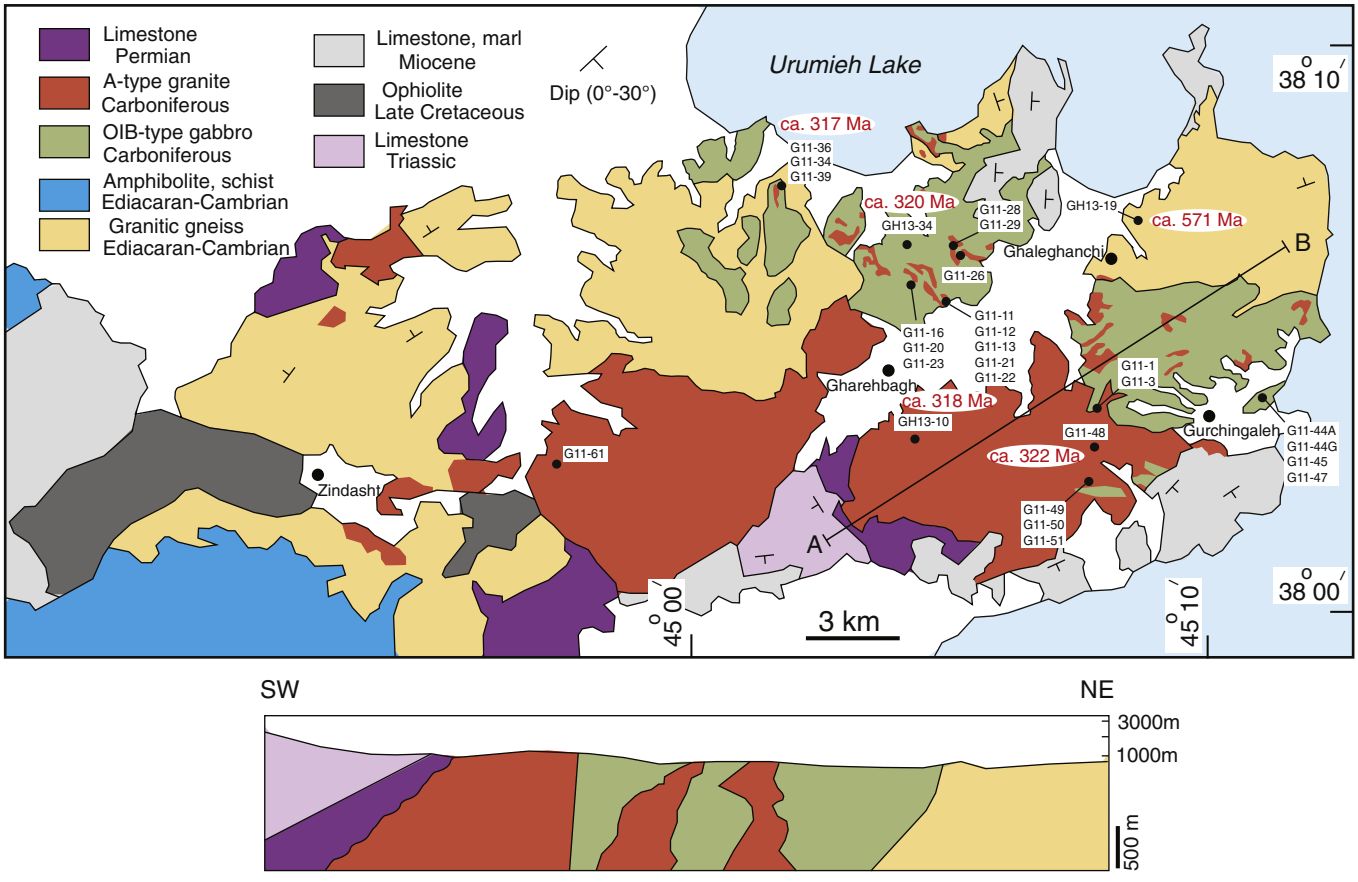

Fig. 2. Geological map of the Ghushchi region (modified after 1/100,000 Ghushchi geological map).

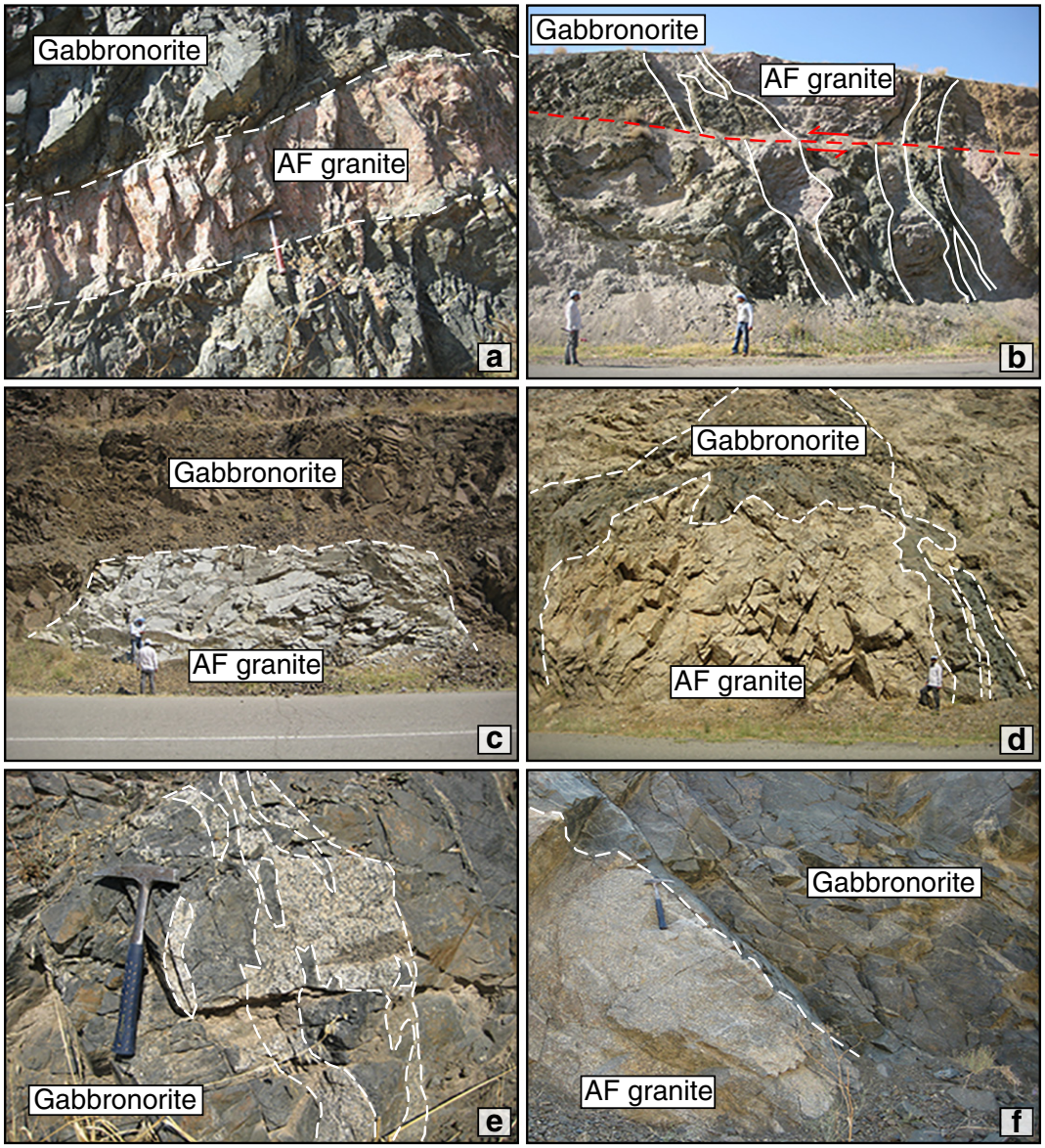

Fig. 3. Field photographs of the Ghushchi complex. a) and b) injection of AF granitic dikes into the gabbronorites. c) and d) stock-like AF granitic intrusions within the Ghushchi gabbronorites. e) Injection of irregular granitic dikelets within the gabbronorites and d) sharp and intrusive contacts between AF granites and gabbronorites.

apatite, and zircon are minor phases. Diabasic dikes include plagioclase phenocrysts and fine-grained clinopyroxene and orthopyroxene.

Plagioclase in gabbronorite is andesine to labradorite (29.1–68.4% An) (Fig. 5a). Orthopyroxene in gabbronorites has Mg# = 0.43–0.61 and low Al_2O_3 (0.3–0.9 wt.%) and TiO_2 (0.1–0.9 wt.%) contents (Supplementary Document 2). These are ferro-hypersthene ($En_{0.42}Fs_{0.55}Wo_{0.03}$ to $En_{0.59}Fs_{0.40}Wo_{0.01}$) (Fig. 5b). Most clinopyroxenes have augite to salite composition (Morimoto et al., 1988) with $En_{0.31}Fs_{0.24}Wo_{0.45}$ to $En_{0.42}Fs_{0.22}Wo_{0.36}$ (Fig. 5d). They have relatively low contents of Al_2O_3 (0.61–1.5 wt.%) and TiO_2 (0.12–0.39 wt.%) but quite high Na_2O (0.21–0.38 wt.%) contents (Supplementary Document 2). Clinopyroxene in OIB-like gabbros should have much higher TiO_2 and high Ti/Al ratio (Loucks, 1990), but the Ghushchi gabbros have low Al and Ti contents, similar to arc-like gabbros. This could be explained by co-precipitation of clinopyroxene and titano-magnetite in gabbronorites, as Ti is highly compatible in titano-magnetite. This also can explain decoupling between low Ti clinopyroxenes but high Ti content in bulk rock (see the next section). Amphibole in gabbronorite has edenite to ferro-edenite composition with 0.8–1.5 wt.% TiO_2. Biotite–phlogopite has 0.41–0.62 Mg# and has high Al_2O_3 (12.8–14.3 wt.%) and TiO_2 (3.8–5.1 wt.%) contents. These mineral compositions indicate that the gabbronorite magma was quite evolved.

In the Plagioclase–Orthopyroxene–Clinopyroxene classification diagram for gabbroic rocks (Streckeisen, 1979), Ghushchi mafic rocks plot in the leuco-gabbronorite field (Fig. 6a).

3.2. Granitic rocks

The Ghushchi granitic rocks consist of orthoclase (mainly perthite; >60–70% vol.), quartz, and minor plagioclase, indicating these are hypersolvus (one feldspar) granites. They have metaluminous compositions, with A/CNK values of <1.1. Perthitic, graphic, micro-granophyric and myrmekitic textures are dominant. Graphic intergrowth of quartz and plagioclase is common (Fig. 4c, e and f). Amphibole, biotite, allanite, zircon, epidote and titanite are minor phases (Fig. 4d). Amphibole-biotite bearing AF syeno-granites show granular texture and contain orthoclase, microcline, quartz, plagioclase and more biotite and amphibole than perthitic AF granites (Fig. 4d). Zircon, titanite and apatite are common. AF granites consist of perthitic orthoclase, microcline, quartz, plagioclase, biotite with minor zircon, amphibole, titanite and epidote.

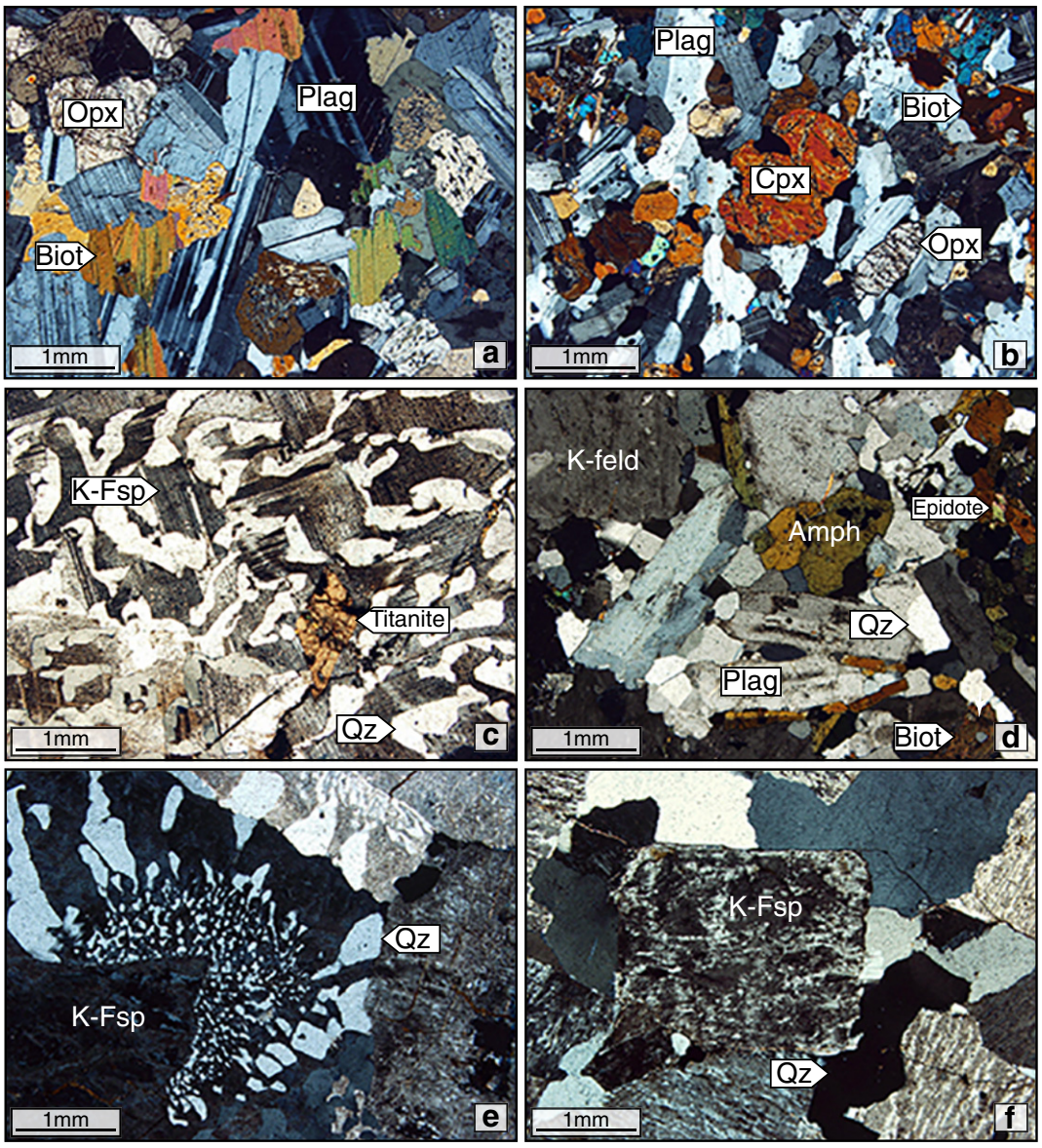

Fig. 4. Microphotographs of Ghushchi rocks. a) and b) orthopyroxene, clinopyroxene, biotite and plagioclase laths in the Ghushchi gabbronorites. c) Graphic texture (intergrowth of quartz, K-feldspar and plagioclase) in AF granites. d) Biotite, amphibole, plagioclase, orthoclase and quartz association in granites. e) granophyric and f) perthitic textures in AF granites.

Aplitic dikes have perthitic orthoclase, quartz with microgranular texture.

Amphibole-biotite syeno-granites are characterized by andesine plagioclase (29.7–43.5 An%) (Fig. 5a); this overlaps the range of gabbronorite plagioclase compositions. Biotite has Mg# = 0.37–0.41 and high Al_2O_3 (13.7–14.1 wt.%) and TiO_2 (3.7–4.6 wt.%) contents. Amphibole in syeno-granites has ferro-edenite to ferro-pargasite composition based on the Leake et al. (1997) classification (Fig. 5c) with high TiO_2 (1.6–1.9 wt.%), Al_2O_3 (7.9–9 wt.%) and Mg# (0.41–0.43) (Supplementary Document 2). In the QAP diagram (Fig. 6b) after Streckeisen (1979), the Ghushchi A-type granites plot predominantly in the field of alkali feldspar (AF) granites, syeno-granites and AF quartz syenites.

4. Whole rock geochemistry

4.1. Major and trace elements

Gabbronorite and diabasic dikes have low SiO_2 (47.4–51.4 wt.%) but moderate Al_2O_3 (14.2–15.7 wt.%) and TiO_2 (1.4–3.1 wt.%) (Supplementary Document 3). Gabbronorites have about 5–7% normative quartz. Their Mg# is low, ranging from 37.9 to 57.8. In a $Na_2O + K_2O$ vs. SiO_2 diagram (Streckeisen, 1979), they plot in the gabbro field (Fig. 6c).

In chondrite-normalized REE diagrams, gabbronorites are characterized by enrichment in light rare-earth elements (LREEs) relative to heavy rare earth elements (HREEs) with $La_{(n)}/Yb_{(n)}$ ~ 6–6.8 (Fig. 7a). They are similar to REE patterns of nearby (and slightly older) Misho gabbronorites. The gabbronorites are enriched in Nb–Ta–Ti and other incompatible elements such as Pb and Zr relative to LREEs. Their trace element signature is broadly similar to that of Ocean Island Basalt (OIB) (Fig. 7b).

AF granites, syeno-granites and aplitic dikes contain 65–80 wt.% SiO_2, 11.2–18.5 wt.% Al_2O_3, 2.2–3.8 wt.% Na_2O and 4.1–8.2 wt.% K_2O (Supplementary Document 3). They are mainly ferroan and fall in the alkali-calcic to calc-alkalic field on the alkali-lime index plot (Frost and Frost, 2011) (Fig. 6d). AF granites have REE-fractionated patterns (Fig. 7c) with enrichment in LREEs relative to HREEs, with $La_{(n)}/Yb_{(n)}$ ~5.3–20.7. Most AF granites show strong negative Eu anomalies, confirming feldspar fractionation. They are depleted in Th, Nb, Ta, Ti, P, Ba and Sr and enriched in Pb, U, Th, K and Zr relative to LREEs (Fig. 7d). Depletion in P, Sr, Ba and Ti could be explained by major

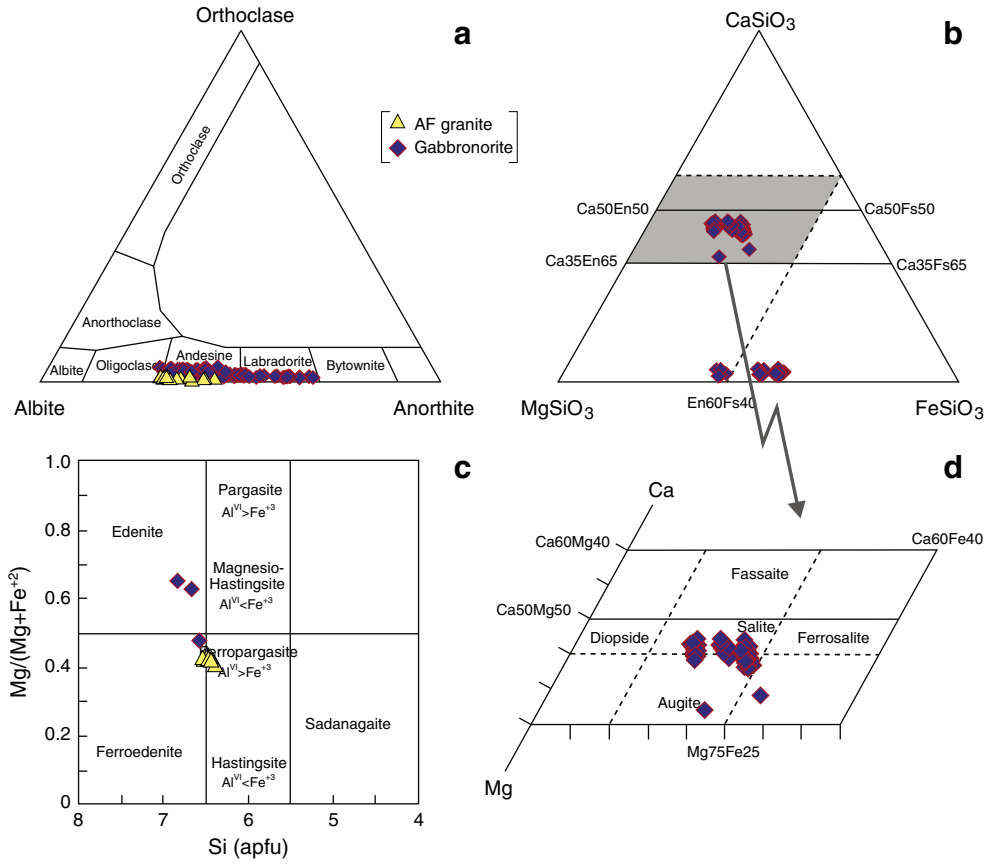

Fig. 5. a) Classification of feldspars on a ternary An–Ab–Or plot (Deer et al., 1992), (b) clinopyroxene classification diagram (Morimoto et al., 1988), and (c) hornblende classification diagram (Leake et al., 1997) of the Ghushchi granites and gabbronorites.

fractionation of apatite, plagioclase and titanomagnetite respectively. Amphibole-biotite bearing syeno-granites, AF-quartz syenite and aplitic dikes also show enrichment in LREEs ($La_{(n)}/Yb_{(n)}$ ~ 2.8–37.7) (Fig. 7e). Interestingly, AF-quartz syenite and aplitic dike contain much less REE and Eu shows strong positive anomalies, suggesting feldspar accumulation. Enrichment in Pb, U, Th, K and Zr and depletion in P, Sr, Ti and Nb–Ta are conspicuous (Fig. 7f).

4.2. Sr–Nd isotopes

Sr–Nd isotopic analyses of the Ghushchi rocks are presented in Supplementary Document 4. The initial $^{87}Sr/^{86}Sr$ calculated at 320 Ma ranges between 0.7033 and 0.7043 for gabbronorites. These rocks contain high Sr abundances (>300 ppm) and low $^{87}Rb/^{86}Sr$ (<0.2) so the modest range in initial $^{87}Sr/^{86}Sr$ found for 4 gabbronorite samples are considered reliable indicators of magmatic compositions. In contrast, A-type granites show a tremendous range of initial $^{87}Sr/^{86}Sr$, from 0.7149 to 0.9217. This large range may be due to very high $^{87}Rb/^{86}Sr$ resulting in imprecise corrections and/or alteration. Excluding all samples with $^{87}Rb/^{86}Sr > 3$ leaves one sample (G11–21), for which an initial $^{87}Sr/^{86}Sr$ of 0.71492 is calculated. Even this is unreasonably high for the observed εNd (320 Ma) ~0 to +4. We conclude that initial $^{87}Sr/^{86}Sr$ in all Ghushchi granitic rocks has been disturbed and do not discuss these further.

The εNd (320 Ma) of the Ghushchi gabbronorites range from +1.3 to +3.4 (Mean = +2.0 ± 1.0) whereas A-type granites show values between −0.08 and 4.07 (Mean = +1.3 ± 1.4; Supplementary Document 4); εNd (320 Ma) for gabbronorite and granite are essentially indistinguishable. T_{DM} Nd model ages (Depaolo, 1981) cluster around 0.57 to 1.6 Ga for Ghushchi rocks, showing an affinity to Cadomian lithosphere, which makes up the continental crust of Iran as well as the immediate host rock.

5. U–Pb zircon geochronology and Hf isotopes

SIMS zircon U–Pb dating was conducted on three AF granite (GH13–10, G11–34 and G11–48), two gabbronorites (GH13–34 and G11–36) and one granitic gneiss (GH13–19) that is the wallrock of the Ghushchi pluton. Sample locations are shown in Fig. 2. Core–mantle structures have been observed for some zircons in CL images. No zircon inheritance exists in the Carboniferous magmas. Analytical data for zircon age data is presented in Supplementary Document 5.

5.1. GH13–34 (gabbronorite)

Zircons from sample GH13–34 are large, mostly >150–200 μm long. In CL images, zircons are characterized by concentric magmatic zoning and inherited cores (Fig. 8a). Fifteen analyses were conducted on the zircons and/or domains. The zircons have low to moderate (201–1210 ppm) U and Th (90–611 ppm) contents, with Th/U ratios between 0.33 and 0.67 (Supplementary Document 5). Common lead is low, value for f_{206} (the proportion of common ^{206}Pb in total measured ^{206}Pb) ranges from 0.06 to 1.1%. Ratios of $^{206}Pb/^{238}U$ and $^{207}Pb/^{235}U$ agree internally within the analytical precision (Fig. 8a), yielding a Concordia age of 319.9 ± 2.5 Ma (MSWD of concordance = 0.028). This age is interpreted as the timing of gabbronorite magma emplacement.

5.2. G11–36 (gabbronorite)

Zircons from sample G11–36 are large, mostly >250 μm long. In CL images, zircons are euhedral to subhedral and characterized by

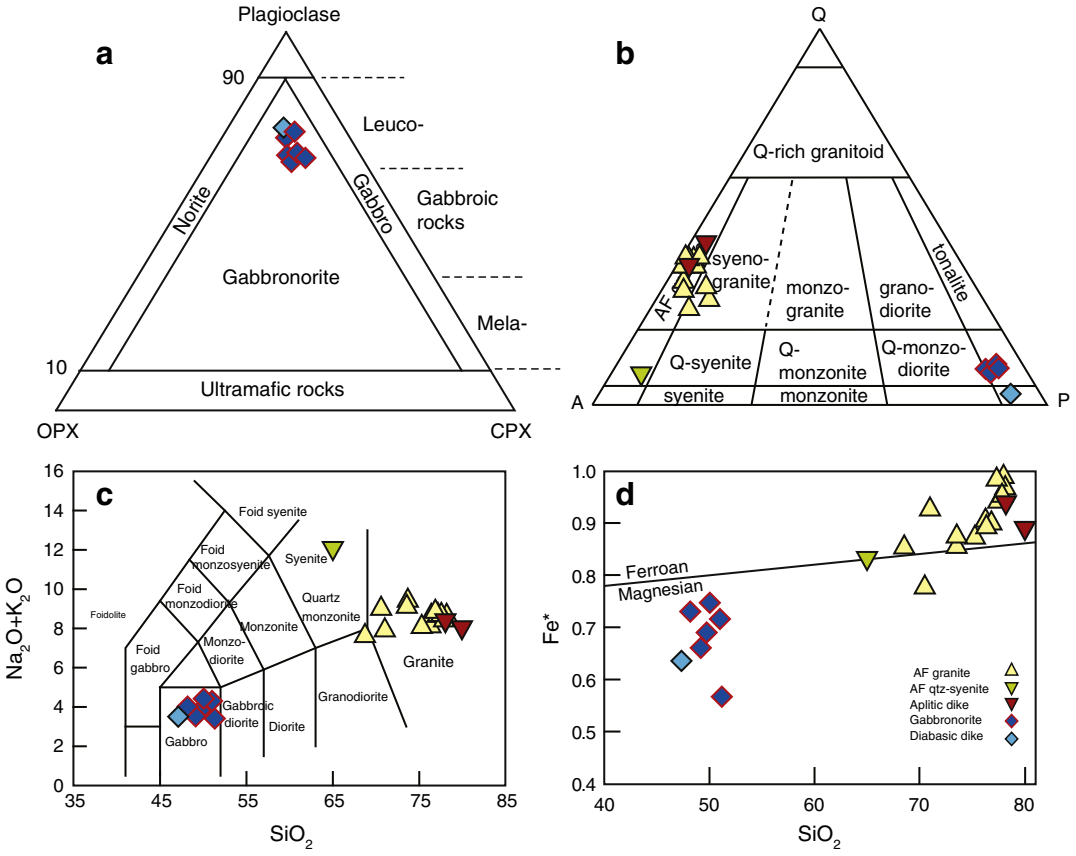

Fig. 6. a) Plagioclase, orthopyroxene (OPX) and clinopyroxene (CPX) classification for Ghushchi mafic rocks. b) Quartz-Alkali feldspar-Plagioclase (QAP) classification diagram for Ghushchi A-type granites. c) $Na_2O + K_2O$ vs. SiO_2 diagram (Streckeisen, 1979) for classification of the Ghushchi rocks. d) (FeO^t/MgO) vs. SiO_2 plot for the Ghushchi rocks (Frost and Frost, 2011).

concentric magmatic zoning (Fig. 8b). Sixteen analyses were conducted on this sample. The zircons have low to moderate (137–1708 ppm) U and Th (64–774 ppm) contents, with Th/U ratios between ~0.3 and 1 (Supplementary Document 5). Value of f_{206} ranges from 0.12 to 0.59%. All analyses have concordant U–Pb ages within analytical errors (Fig. 8b), yielding a Concordia age of 316.8 ± 2.3 Ma (MSWD of concordance = 0.03). This is interpreted as the crystallization age for sample G11–36.

5.3. GH13–10 (AF granite)

Zircon grains in sample GH13–10 are euhedral to subhedral with lengths of 100 to 200 μm (Fig. 8c). They show long to short prismatic shapes. In CL images, most grains show magmatic zoning (Fig. 8c). Core and rim structures are present. A total of 18 spots were analyzed (Supplementary Document 5). The zircons have variable, but mostly high U (546–1639 ppm) and Th (267–1165 ppm) contents, resulting in moderately high Th/U (0.39–0.73). Most zircons are low in common Pb, with value of $f_{206} < 0.7\%$ (Supplementary Document 5). All but one (spot@12) analysis is concordant within analytical errors (MSWD of concordance = 0.49) (Fig. 8c). A Concordia age of 318.4 ± 2.3 Ma is obtained, which is interpreted as the crystallization age for sample GH13–10. Spot @12 was an analysis on a core, giving a slightly older age of 392 Ma.

5.4. G11–34 (AF granite)

Zircons in sample G11–34 are euhedral, 100 to 200 μm long (Fig. 8d). They show long to short prismatic shapes. In CL images, most grains show magmatic zoning. A total of 24 spots were analyzed (Supplementary Document 5). The zircons have variable, but mostly high U (111–1885 ppm) and Th (48–623 ppm) contents, resulting in moderately low to high Th/U (0.08–0.67). Common Pb is low, with value of f_{206} between 0.02 and 0.7 (Supplementary Document 5). Most analyses are concordant within analytical errors. They give a concordia age of 317.3 ± 1.9 Ma (MSWD of concordance = 0.024) (Fig. 8d), interpreted as the time of granite emplacement.

5.5. G11–48 (AF granite)

Zircons in sample G11–48 are subhedral, with lengths of 100–150 μm (Fig. 8e). In CL images, most grains show magmatic zoning (Fig. 8e). A total of 19 spots were analyzed (Supplementary Document 5). Among them, nine grains have high U contents (>2000 ppm), which could yield unrealistic older or younger ages compared to the normal zircons (Li et al., 2013). The remaining ten zircons have variable U (162–1878 ppm) and Th (69–658 ppm) contents, and Th/U (0.05–1.4). They are low in common Pb content, with f_{206} value of 0.1–0.7% (Supplementary Document 5). These ten analyses are concordant within analytical errors, yielding a concordia age of 322.0 ± 2.9 Ma (MSWD of concordance = 0.42) (Fig. 8e). This is interpreted as the best estimate of the crystallization age of the granite magma.

5.6. GH13–19 (Granitic gneiss)

Zircons from sample GH13–19 are medium-grained (80–150 μm) and euhedral to anhedral, with concentric magmatic zoning. Inherited cores are visible in some grains. Fifteen analyses were conducted on zircons from this sample. The zircons have low to medium (114–890 ppm) U and Th (28–147 ppm) contents with Th/U ratios between 0.09 and 0.94 (Supplementary Document 5). Common lead is low, with f_{206} value ranging from 0.04 to 0.59. Thirteen analyses have concordant

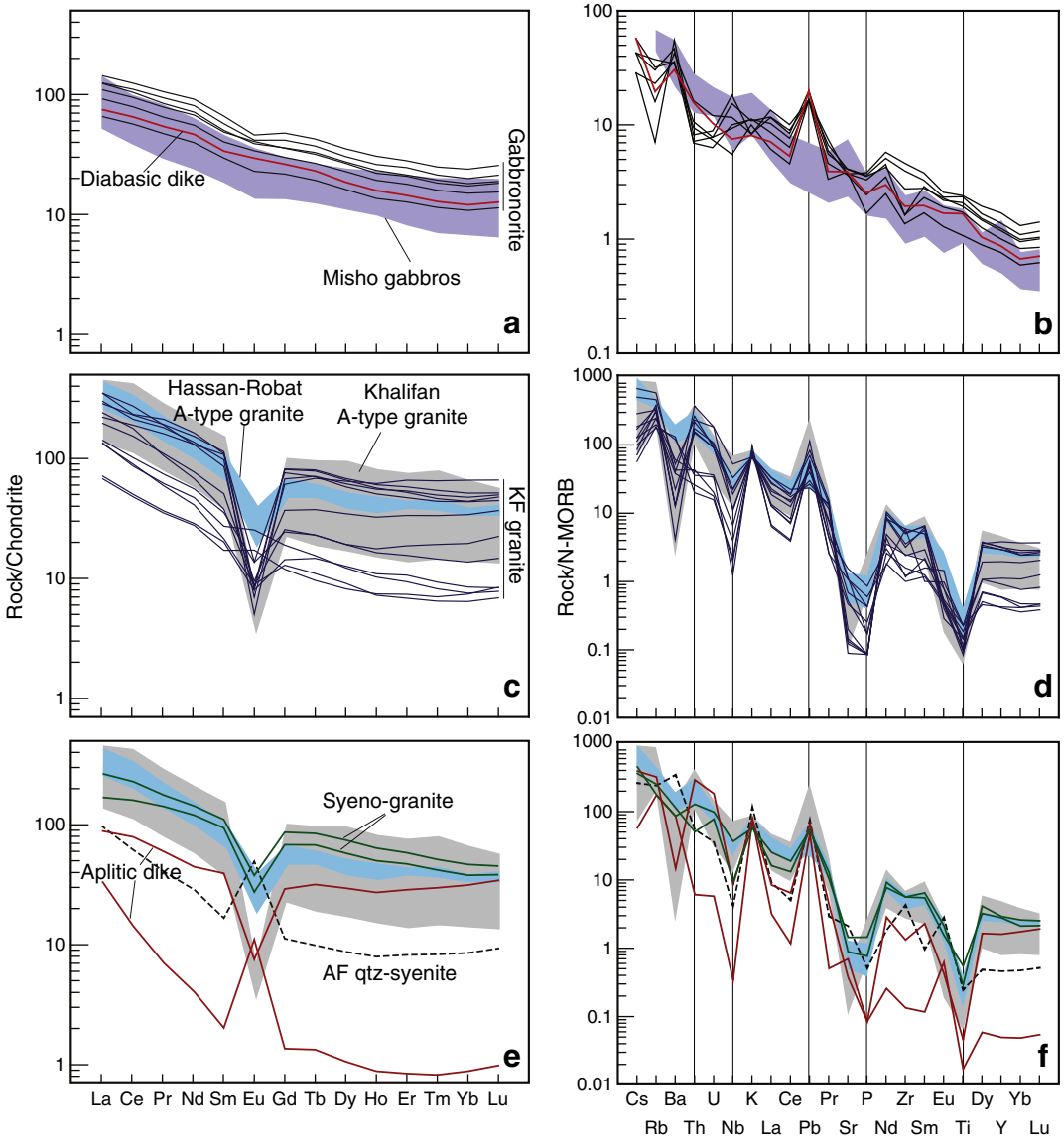

Fig. 7. Chondrite-normalized rare earth elements and N-MORB-normalized trace element patterns for the Ghushchi gabbronorites and granites. Data for Khalifan A-type granites from Bea et al. (2011), Hassan-Robat A-type granites from Alirezaei and Hassanzadeh (2012a) and Misho gabbros from Saccani et al. (2014).

$^{206}Pb/^{238}U$ and $^{207}Pb/^{235}U$ ratios within the analytical precision (Fig. 8f), yielding a concordia age of 571.4 ± 4.5 Ma (MSWD of concordance = 0.097). This is interpreted as the crystallization age of granitic protolith. Spots @6 and @18 are from xenocrystic zircon and inherited core respectively, showing older ages of ca. 686 and 672 Ma.

5.7. Zircon Hf isotopes

The εHf(t) value for zircons from Ghushchi granites and gabbronorites range from +1.7 to +6.2 and +0.94 to +6.5 (Fig. 9). T_{DM1} age (single-stage Hf-isotope model age assuming that the sample was derived from depleted mantle) varies from 1.2 to 1.6 Ga for granites and 1.2–1.7 Ga for gabbronorites whereas T_{DM2} (two-stage Hf-isotope model age assuming that the sample was derived via the lower crust following derivation from depleted mantle) range between 0.8 and 1.1 Ga for both granites and gabbronorites (Fig. 9; Supplementary Document 6). The similarities in model ages for both gabbronorites and granites have been issued from a similar source and are spatially and temporally co-genetic. The εHf(t) value for zircon of Cadomian granitic gneiss is quite variable and varies between −2.8 and +8.9. T_{DM1} and T_{DM2} for granitic gneisses range from 1 to 2.2 and 0.8 to 1.5, respectively.

6. Discussion

6.1. Implication of ages for the Ghushchi complex

Our zircon U–Pb zircon dating shows indistinguishable ages of 317–320 Ma for gabbronorite and 317–322 Ma for granite. Thus, the Ghushchi bimodal magmatic suites were emplaced synchronously at ca. 320 Ma. These are similar to other ages available on similar plutons in NW Iran including Khalifan (ca. 315 Ma) (Bea et al., 2011), Misho (ca. 357 Ma) (Saccani et al., 2014) and Heris (ca. 306 Ma) (Advay and Ghalamghash, 2011), but older than the Hassan-Robat A-type granites (ca. 288 Ma) from Sanandaj–Sirjan Zone (Alirezaei and Hassanzadeh, 2012). The granitic gneiss host of the Ghushchi complex is dated at 571.4 ± 4.5 Ma (Ediacaran–Cambrian), similar to widespread 500–600 Ma Cadomian crust of Iran (Shafaii Moghadam et al., 2015).

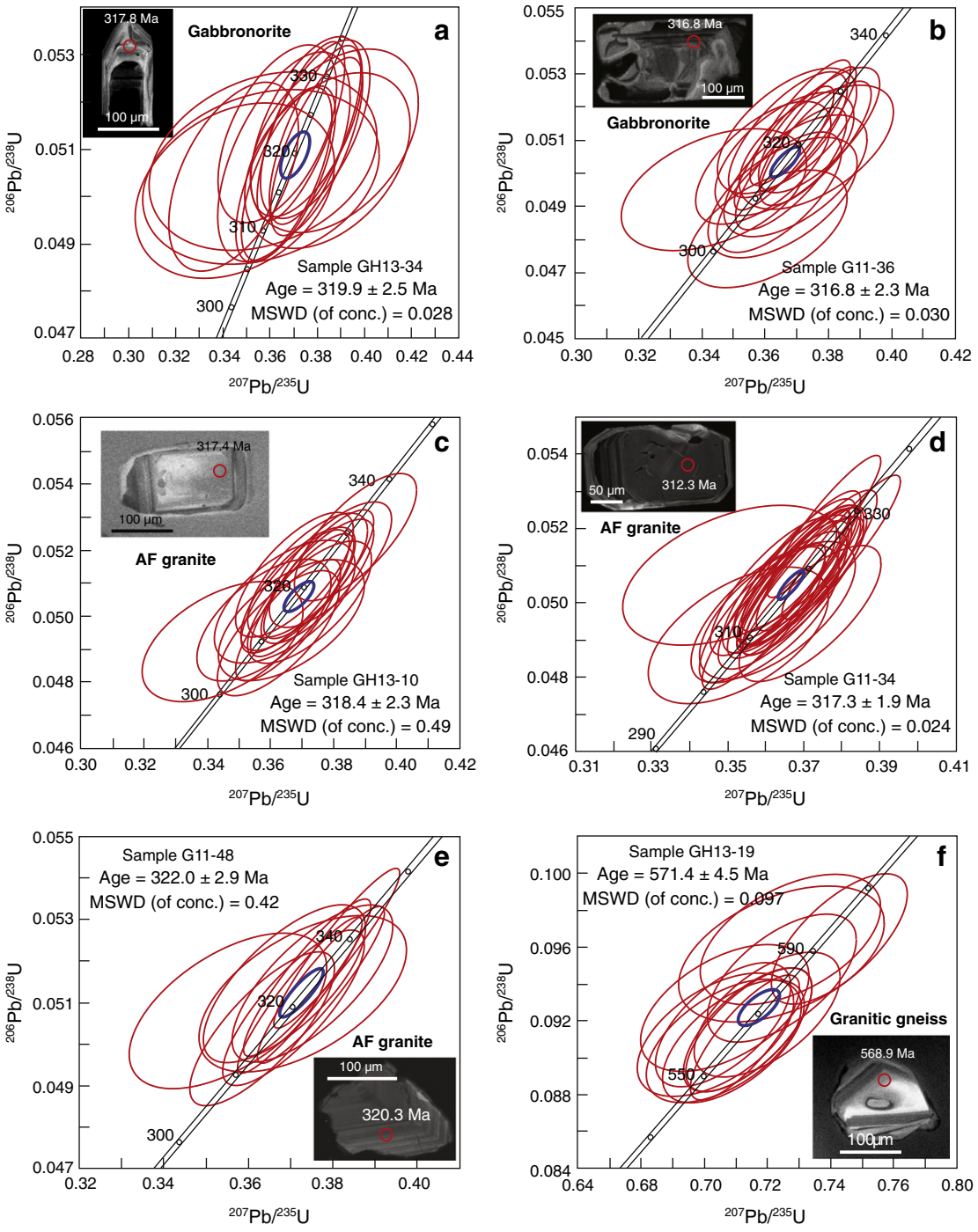

Fig. 8. Representative cathodoluminescence images and conventional (Wetherill) concordia diagrams for the Ghushchi granites, gabbronorites and host granitic gneiss.

6.2. Classification of Ghushchi complex rocks

Ghushchi gabbronorites are fractionated, and their quartz-normative nature indicates a broadly tholeiitic suite but one that was enriched in large ion lithophile and light rare earth elements. The parental magma that was similar in terms of incompatible trace elements to OIB-type rocks including LREEs and Nb–Ta enrichments and high concentrations of incompatible trace elements (Fig. 7a and b). These geochemical characteristics along with their low εNd with strong Cadomian affinities indicate that some or all of the gabbronorites have a lower continental crust and/or sub-continental mantle source.

Ghushchi granites are hypersolvus (one feldspar) granites. They have metaluminous compositions. They show strong Fe-enrichment, indicative of derivation from a broadly tholeiitic suite. Ghushchi granites have chemical compositions that are typical of A-type granites, including high $K_2O + Na_2O$, Zr, total FeO^t/MgO and Ga/Al ratios and low CaO, Sr, and Eu abundances. In discrimination diagrams of $Na_2O + K_2O$ and Zr vs. 10000Ga/Al, they plot in the A-type granite field of Whalen et al., 1987) (Fig. 10). Furthermore, in the Nb–Y–Zr/4, Nb–Y–3 × Th, Nb–Ce–Y and Nb–Y–3 × Ga diagrams, most samples fall within the field of A_2-type granites (Eby, 1992) (Fig. 11) globally interpreted as representing A-type magmas derived from lower continental crust.

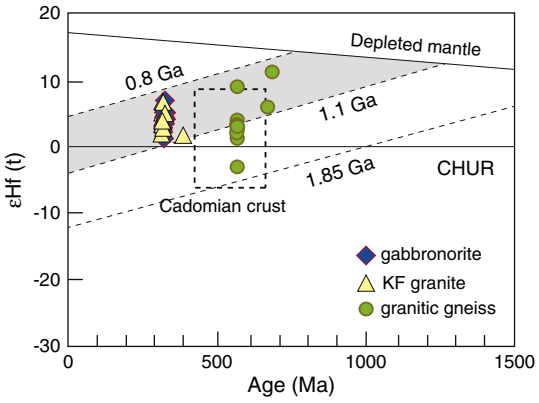

Fig. 9. Zircon εHf(t) vs. U–Pb ages for the Ghushchi gabbronorites, granites and granitic gneiss.

The higher Y content of the A-type granites may also relate to the presence of modal calcic amphiboles.

6.3. Petrogenesis

We know that Ghushchi alkali granite and gabbronorite magmas co-existed in the same magma reservoir at ~320 Ma. We know from indistinguishable Nd and Hf isotopic compositions that only a single source was involved, but we do not understand what was the relationship between mafic and felsic components. Did granite magmas form by fractionation of gabbronorite magma? Or are both gabbronorites and granites melts of the same source?

A-type granites worldwide can be attributed to three main petrogenetic scenarios, including (1) extreme differentiation of mantle-derived tholeiitic or alkaline basaltic magma precursor (Mushkin et al., 2003; Turner et al., 1992); (2) partial melting of crustal rocks (Bonin, 2007; Huang et al., 2011; King et al., 1997; Landenberger and Collins, 1996); and (3) combined crustal and mantle sources, in the form either of crustal assimilation and fractional crystallization (AFC) of mantle-derived magmas, or mixing between mantle-derived and crustal magmas (Kemp et al., 2005; Yang et al., 2006; Zhang et al., 2012). Isotopic identity between Ghushchi granite and gabbronorite makes it unlikely that the two are different mixtures of crustal and mantle melts. However, the Ghushchi gabbronorites are evolved rocks with compositions that could have been affected by crustal assimilation or magma mingling. Crustal assimilation or magma mingling for gabbronorites is not confirmed by zircon Hf isotopes or bulk rock Nd isotopes and inherited zircons. For mingling, the zircon εHf of gabbronorites is similar to granites and differs from igneous rocks formed by mixing of sediment melts with mantle-derived magmas, which commonly show greater isotopic variability (e.g., Griffin et al., 2002; Kemp et al., 2007).

Ghushchi granites A_2 granites show some involvement of ~680 Ma crust as indicated by inherited zircons. A diversity of crustal protoliths is envisaged to generate A_2 magmas, including dry residual granulitic or charnockitic lower crust (Collins et al., 1982; Landenberger and Collins, 1996) and quartzo-feldspathic igneous rocks (Patiño Douce, 1997). Generation via melting of residual granulitic lower crust could not explain the genesis of A-type granites, due to the contradiction between major element compositions expected from partial melts of such a depleted source and A-type granitic melts (Creaser et al., 1991), although lower crust granulites can produce A-type granites by low melt fractions. Dehydration melting of a quartzo-feldspathic igneous source also yields calc-alkalic peraluminous granites (Bonin et al., 1998). It is not clear how melting such materials would generate gabbronorite magma as well.

Prominent Eu and Sr depletions in the Ghushchi A-type granites suggest an important role for feldspar during melting and/or fractionation. The flat HREE patterns point to a pyroxene-rich but garnet-absent residue or fractionate. These geochemical behaviors could be explained by melting of a charnockite with oceanic crust affinity. However, moderately positive bulk rock Nd and zircon Hf isotopic signatures in gabbronorites are inconsistent with an asthenospheric source but could be generated by melting of Cadomian subcontinental mantle lithosphere or juvenile crust. Melting of the same material could be another scenario for the genesis of the Ghushchi magmas but if so, how to explain such different major and trace element compositions? And why would melting of the same rock generate two different magma compositions, both gabbronorite and granite?

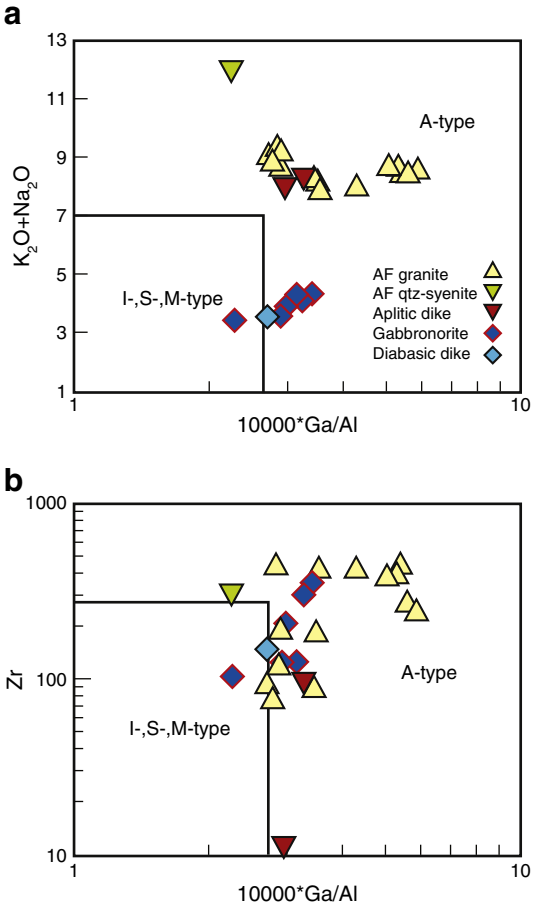

Fig. 10. $K_2O + Na_2O$ and Zr vs. 10,000 Ga/Al diagrams (Whalen et al., 1987) for the subdivision of the Ghushchi granitic rocks. For comparison, gabbronorites are also plotted.

Part of the petrogenetic uncertainty is that we do not know whether the entire composite intrusion is exposed or if there is a missing part, which is likely to be more mafic. Gabbronorites are characterized by high Nb–Ta concentrations and follow the mantle array in a Th/Yb vs. Ta/Yb diagram (Fig. 12a) whereas granites have higher Th contents. Granites also have variable Nb + Y values, plotting both in Volcanic Arc Granite (VAG) and Within Plate Granite (WPG) fields (Fig. 12b). The gabbronorites are similar to OIB type rocks whereas granites are similar to continental crust by having a higher U content (Fig. 12c). Higher U and Th abundances of granites reflect the highly evolved characteristics of these rocks, as Th and U are highly incompatible and concentrate in residual melts. Niobium depletion of the granites could also be explained by fractionation of Nb-rich phases such as amphibole, titanite and rutile. Given the occurrence of isotopically indistinguishable and similarly aged mafic gabbronorites, it is appealing to envision that a mafic magma progenitor produced the A-type granites via extreme crystal fractionation of the same magma. As is testified by $La_{(n)}/Yb_{(n)}$ vs. La and $^{143}Nd/^{144}Nd$ vs. SiO_2 diagrams (Fig. 12e and f), the A-type granites and coeval gabbronorites define a trend that is consistent with fractional crystallization without AFC. On the other hand, the lack

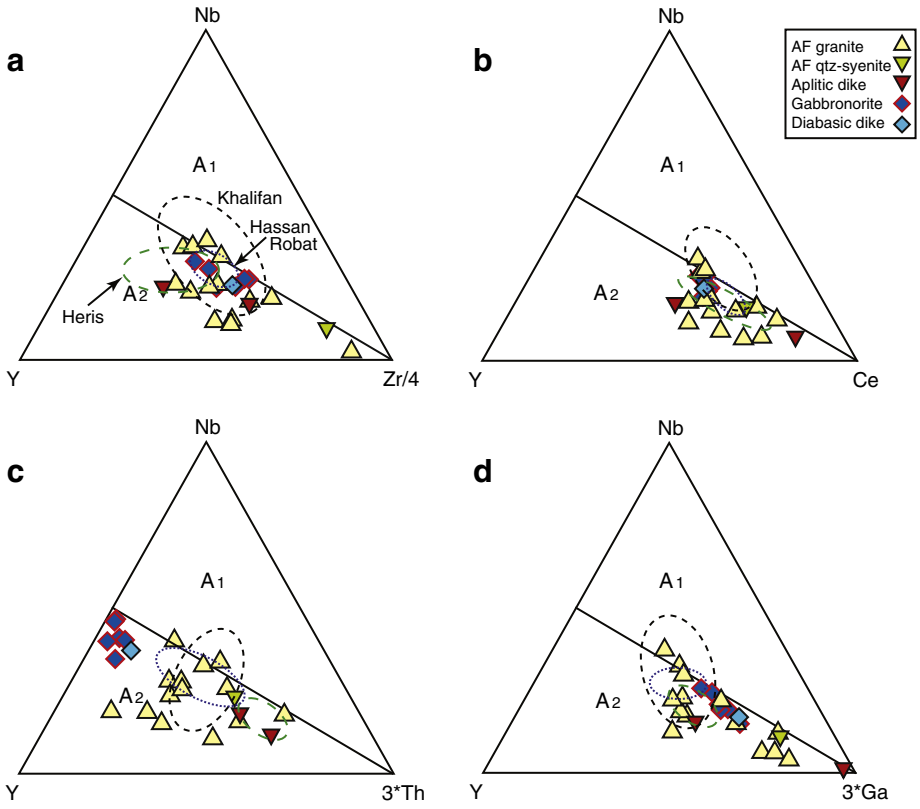

Fig. 11. Nb–Y–Zr/4, Nb–Y–3 × Th, Nb–Ce–Y and Nb–Y–3 × Ga diagrams (Eby, 1992) for classification of Ghushchi granites. Data for Khalifan A-type granites from Bea et al. 2011), Heris from Advay and Ghalamghash (2011) and Hassan-Robat A-type granites from Alirezaei and Hassanzadeh (2012a). For comparison, gabbronorites are also plotted.

of layering in the gabbronorites argues against crystal fractionation, although small fractions of liquid can be expelled from gabbroic magmas without leaving a layered structure. Nevertheless, the nearly sub-equal volume of gabbronorite and granite makes it very difficult to accept that felsic and mafic members are related by simple fractional crystallization.

We may not yet be able to explain the detailed petrogenesis of the Ghushchi rocks, but it clearly involved extension, mantle upwelling and rising asthenosphere associated with rifting to open Tethys. This would involve melting of lithospheric mantle to produce gabbronorites or now-hidden more primitive melts from which gabbronorite evolved by fractionation. Extreme differentiation of a sufficiently large volume of hidden mafic melts could have generated A-type granites. While it is likely Ghushchi granites and gabbronorites are petrogenetically related, we cannot entirely exclude other possibilitie such as (1) re-melting of pre-existing crustal components (with similar bulk rock Nd and zircon Hf isotopes to that of the gabbronorites) and (2) A-type granite melts were generated independently from gabbronorite melts. The heat and volatiles transferred from basaltic magma may have been critical factors in many situations where partial melting of pre-existing old crust (and/or new basaltic crust) occurs (e.g., Annen and Sparks, 2002). These processes could explain the different geochemical features such as high Nb/U and low Th/Yb ratios in gabbronorites and "arc-like" signatures for granites.

It is also possible that Ghushchi composite igneous complex formed by large-scale silicate liquid immiscibility of an originally homogeneous magma (e.g. Charlier et al., 2011). Such a simple interpretation is broadly consistent with the geochronological and isotopic evidence. Evidence for silicate liquid immiscibility is increasingly reported and this phenomenon results in two magmas: Fe-rich mafic and Fe-poor felsic (Jakobsen et al., 2005). An interpretation of liquid immiscibility for the Ghushchi complex is favored by the high-Fe nature (10–15 wt.% $Fe_2O_3^T$) of the gabbronorites, although these are not as Fe-rich as some mafic end-members, for example those reported by Jakobsen et al. (2005). Mineralogically, the gabbronorites are similar to apatite-bearing, evolved cumulate ferrogabbros of the Sept Iles layered intrusion (Canada) which are thought to have crystallized from immiscible Fe-rich and Si-rich silicate melts that segregated in a slow-cooling magma chamber (Namur et al., 2012). We note that liquid immiscibility usually produces large geochemical variability in resultant ferrogabbros (Namur et al., 2011, 2012) but the Ghushchi gabbros are geochemically homogeneous.

We recognize that the above discussion is inconclusive and that further careful studies designed to address the precise relationship between gabbronorite and alkali granite are needed. These studies should include fieldwork to identify possible layering in the gabbronorite, the original orientation of the body (how much has it been tilted?); the nature and significance of the granite–gabbronorite contact; gravity and magnetic studies (is there evidence of dense, Fe-rich mass beneath (to the NE of) the exposed gabbronorite?), and careful studies of melt inclusions in apatite and other minerals to better constrain the composition of the parental magma. Other intrusions of similar age in the region should be examined to see if there are other examples of composite plutons from which petrogenetic clues can be extracted.

6.4. Geodynamic implications

Middle and Late Paleozoic (420 to 320 Ma) igneous rocks in central and western Europe are related to Rheic Ocean subduction and collision between Gondwana and Eurasia, whereas igneous rocks farther east reflect rifting and ocean opening (Kroner and Romer, 2013). Cadomian terranes in Iran are thought to be fragments from rifting of Gondwana to open Neotethys during Late Paleozoic time, and these may preserve evidence of this rifting as well as evidence for collision of rifted Cadomian fragments with Eurasia (Shafaii Moghadam and Stern, 2014). NW Iran is thus a key region where Late Paleozoic igneous

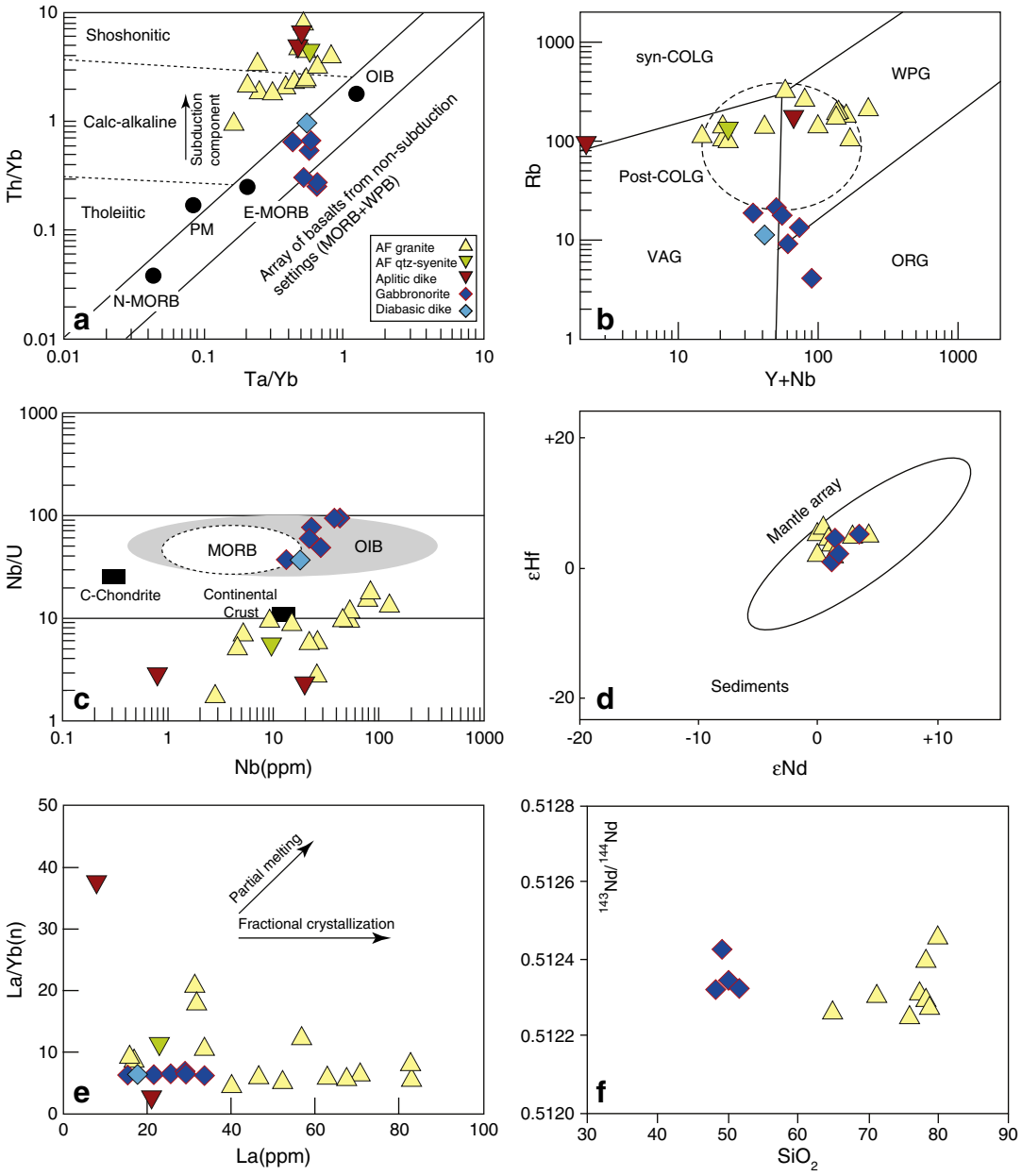

Fig. 12. a) Th/Yb vs. Ta/Yb (Pearce and Peate, 1995), b) Rb vs. Y + Nb (Pearce et al., 1984), c) Nb/U vs. Nb, d) zircon εHf(t) vs. bulk rock εNd(t), e) $La_{(n)}/Yb_{(n)}$ vs. La and f) $^{143}Nd/^{144}Nd$ vs. SiO_2 for Ghushchi granites and gabbronorites.

rocks can be used to help reconstruct the tectonic evolution of north Gondwana and SW Eurasia during Late Paleozoic time.

Evidence of Carboniferous deformation and magmatism is increasingly being recognized in Iran and in northern Arabia. In northern Arabia there are two major angular regional unconformities — one is Late Silurian–Early Devonian (sometimes called "Caledonian") and the other is mid-Carboniferous (commonly called "Hercynian"). In Syria these unconformities merge (Brew et al., 2001) whereas in northern Iraq they are separated by a section that includes marine sediments (Al-Hadidy, 2007). What is the significance of the crustal movements that Carboniferous angular unconformities record? It has long been recognized that northern Arabia was affected by Carboniferous deformation that has been related to the Hercynian orogeny in Europe (Faqira et al., 2009; Husseini, 1992; Kohn et al., 1992; Konert et al., 2002; Stern et al., 2014). Recent studies call this interpretation into question, for example the identification of Carboniferous igneous rocks beneath southern Syria (Stern et al., 2014) and evidence of pre-Permian normal faults in the High Zagros, interpreted to be thermal, not tectonic, in origin (de Lamotte et al., 2013; Tavakoli-Shirazi et al., 2013). Certainly Ghushchi A-type granites and geochemically similar Khalifan A-type granite in NW Iran can be related to Mid- to Late Carboniferous crustal movements, and the Hassan-Robat Permian A-type granite may also be related. The compositional characteristics of the bimodal Ghushchi complex are most consistent with magmatic activity in an extensional tectonic environment. This extension may have occurred during rifting of Cadomian fragments – also known as Cimmeria – away from northern Gondwana. This opened Neotethys and rifted fragments traveled north to collide with Eurasia, closing Paleotethys and producing the Permian–Triassic suture in northern Iran (Shafaii Moghadam and Stern, 2014). Ghushchi igneous rocks may have formed in association with this ~320 Ma rifting episode. Further studies are needed to better understand the significance of Carboniferous igneous rocks, structures, and unconformities in Anatolia and Persia. It may be that alignment of Carboniferous igneous rocks could reveal an ancient rift

zone and provide important new insights into the tectonomagmatic evolution of northern Gondwana and SW Asia.

7. Conclusions

SIMS zircon U–Pb dating constrains a Carboniferous crystallization age for gabbronorite and granite from the Ghushchi complex (NW Iran). These granites exhibit the geochemical character of A-type magmas whereas gabbronorites have OIB-type signature. Moderately high bulk rock εNd and zircon εHf isotopic signatures for gabbronorites and granites show derivation from an enriched mantle source, perhaps the subcontinental mantle. Similar bulk rock εNd and zircon εHf for gabbronorites and A-type granites and also similarity in U–Pb zircon ages indicate that these rocks are co-genetic and were little affected by ~570 Ma Cadomian crust they were emplaced into. The Ghushchi complex is further evidence for extensional tectonics and rifting of Cadomian fragments away from northern Gondwana during early phases of Neotethys opening, ~320 Ma.

Supplementary data to this article can be found online at http://dx.doi.org/10.1016/j.lithos.2014.11.009.

Acknowledgements

Thanks to Moujahed Al-Husseini for comments about the "Hercynian unconformity" in Arabia, and to Andreas Kronz for providing analytical support at the EMP. We are very grateful to Antonio Castro and an anonymous reviewer for their constructive reviews of the manuscript. Editorial suggestions by Sun-Lin Chung are appreciated. This research was supported by the "Strategic Priority Research Program (B)" of the Chinese Academy of Sciences (Grant no. XDB03010800) to XHL and the State Key Laboratory of Lithospheric Evolution, IGG-CAS to HSM. All logistical supports during field studies came from Damghan University.

References

Advay, M., Ghalamghash, J., 2011. Petrogenesis and U–Pb dating zircon of granites of Heris (NW of Shabestar), eastern Azerbaigan province. Iranian Journal Crystallography Mineralogy 4, 633–648.

Aharipour, R., Moussavi, M.R., Mosaddegh, H., Mistiaen, B., 2010. Facies features and paleoenvironmental reconstruction of the Early to Middle Devonian syn-rift volcano-sedimentary succession (Padeha Formation) in the Eastern-Alborz Mountains, NE Iran. Facies 56, 279–294.

Alavi, M., 1991. Sedimentary and structural characteristics of the Paleo-Tethys remnants in northeastern Iran. Geological Society of America Bulletin 103, 983–992.

Al-Hadidy, A.H., 2007. Paleozoic stratigraphic lexicon and hydrocarbon habitat of Iraq. GeoArabia 12, 63–130.

Alirezaei, S., Hassanzadeh, J., 2012. Geochemistry and zircon geochronology of the Permian A-type Hasanrobat granite, Sanandaj–Sirjan belt: a new record of the Gondwana break-up in Iran. Lithos 151, 122–134.

Annen, C.S., Sparks, R.S.J., 2002. Effects of repetitive emplacement of basaltic intrusions on thermal evolution and melt generation in the crust. Earth and Planetary Science Letters 203, 937–955.

Bea, F., Mazhari, A., Montero, P., Amini, S., Ghalamghash, J., 2011. Zircon dating, Sr and Nd isotopes, and element geochemistry of the Khalifan pluton, NW Iran: evidence for Variscan magmatism in a supposedly Cimmerian superterrane. Journal of Asian Earth Sciences 40, 172–179.

Berberian, M., King, G.C.P., 1981. Towards a paleogeography and tectonic evolution of Iran. Canadian Journal of Earth Sciences 18, 210–265.

Bonin, B., 2004. Do coeval mafic and felsic magmas in post-collisional to within-plate regimes necessarily imply two contrasting, mantle and crustal, sources? A review. Lithos 78, 1–24.

Bonin, B., 2007. A-type granites and related rocks: evolution of a concept, problems and prospects. Lithos 97, 1–29.

Bonin, B.L., Azzouni-Sekkal, A., Bussy, F., Ferrag, S., 1998. Alkali-calcic and alkaline post-orogenic (PO) granite magmatism: petrologic constraints and geodynamic settings. Lithos 45, 45–70.

Boulin, J., 1991. Structures in Southwest Asia and evolution of the eastern Tethys. Tectonophysics 196, 211–268.

Brew, G., Barazangi, M., Al-Maleh, A.K., Sawaf, T., 2001. Tectonic and geologic evolution of Syria. GeoArabia 6, 573–616.

Charlier, B., Namur, O., Toplis, M.J., Schiano, P., Cluzel, N., Higgins, M.D., Auwera, J.V., 2011. Large-scale silicate liquid immiscibility during differentiation of tholeiitic basalt to granite and the origin of the Daly gap. Geology 39, 907–910.

Chiu, H.-Y., Chung, S.-L., Zarrinkoub, M.H., Mohammadi, S.S., Khatib, M.M., Iizuka, Y., 2013. Zircon U–Pb age constraints from Iran on the magmatic evolution related to Neotethyan subduction and Zagros orogeny. Lithos 162–163, 70–87.

Collins, W.J., Beams, S.D., White, A.J.R., Chappell, B.W., 1982. Nature and origin of A-type granites with particular reference to southeastern Australia. Contributions to Mineralogy and Petrology 80, 189–200.

Creaser, R.A., Price, R.C., Wormald, R.J., 1991. A-type granites revisited — assessment of a residual-source model. Geology 19, 163–166.

de Lamotte, D.F., Tavakoli-Shirazi, S., Leturmy, P., Averbuch, O., Mouchot, N., Raulin, C., Leparmentier, F., Blanpied, C., Ringenbach, J.C., 2013. Evidence for Late Devonian vertical movements and extensional deformation in northern Africa and Arabia: integration in the geodynamics of the Devonian world. Tectonics 32, 107–122.

Deer, W.A., Howie, R.A., Zussman, J., 1992. An introduction to the Rock Forming Minerals, 2nd ed. Longman Group Ltd, Harlow (712 pp).

Depaolo, D.J., 1981. Trace-element and isotopic effects of combined wallrock assimilation and fractional crystallization. Earth and Planetary Science Letters 53, 189–202.

Dokuz, A., Uysal, I., Kaliwoda, M., Karsli, O., Ottley, C.J., Kandemir, R., 2011. Early abyssal- and late SSZ-type vestiges of the Rheic oceanic mantle in the Variscan basement of the Sakarya Zone, NE Turkey: implications for the sense of subduction and opening of the Paleotethys. Lithos 127, 176–191.

Eby, G.N., 1990. The a-type granitoids: a review of their occurrence and chemical characteristics and speculations on their petrogenesis. Lithos 26, 115–134.

Eby, G.N., 1992. Chemical subdivision of the A-type granitoids: petrogenetic and tectonic Implications. Geology 20, 641–644.

El Dabe, M.M., 2013. A geochemical tectonomagmatic classification of the A-type granitoids based on their magma types and tectonic regimes. Arabian Journal of Geosciences http://dx.doi.org/10.1007/s12517-013-1195-8.

Faqira, M., Rademakers, M., Afifi, A.M., 2009. New insights into the Hercynian Orogeny, and their implications for the Paleozoic hydrocarbon system in the Arabian plate. GeoArabia 14, 199–228.

Frost, C.D., Frost, B.R., 2011. On Ferroan (A-type) granitoids: their compositional variability and modes of origin. Journal of Petrology 52, 39–53.

Griffin, W.L., Wang, X., Jackson, S.E., Pearson, N.J., O'Reilly, S.Y., Xu, X.S., Zhou, X.M., 2002. Zircon chemistry and magma mixing, SE China: in-situ analysis of Hf isotopes, Tonglu and Pingtan igneous complexes. Lithos 61, 237–269.

Huang, H.Q., Li, X.H., Li, W.X., Li, Z.X., 2011. Formation of high $\delta^{18}O$ fayalite-bearing A-type granite by high-temperature melting of granulitic metasedimentary rocks, southern China. Geology 39, 903–906.

Husseini, M.I., 1992. Upper Paleozoic tectono-sedimentary evolution of the Arabian and adjoining plates. Journal of the Geological Society of London 149, 419–429.

Jakobsen, J.K., Veksler, I.V., Tegner, C., Brooks, C.K., 2005. Immiscible iron- and silica-rich melts in basalt petrogenesis documented in the Skaergaard intrusion. Geology 33, 885–888.

Kemp, T., Paterson, B., Hawkesworth, C., 2005. A coupled Lu–Hf and O isotope in zircon approach to granite genesis. Geochimica et Cosmochimica Acta 69 (Supplement), A243.

Kemp, A.I.S., Hawkesworth, C.J., Foster, G.L., Paterson, B.A., Woodhead, J.D., Hergt, J.M., Gray, C.M., Whitehouse, M.J., 2007. Magmatic and crustal differentiation history of granitic rocks from Hf–O isotopes in zircon. Science 315, 980–983.

King, P.L., White, A.J.R., Chappell, B.W., Allen, C.M., 1997. Characterization and origin of aluminous A-type granites from the Lachlan Fold Belt, Southeastern Australia. Journal of Petrology 38, 371–391.

Kohn, B.P., Eyal, M., Feinstein, S., 1992. A major Late Devonian–Early Carboniferous (Hercynian) thermotectonic event at the NW margin of the Arabian–Nubian shield: evidence from zircon fission track dating. Tectonics 11, 1018–1027.

Konert, G., Al-Hajri, S.A., Al Naim, A.A., Afifi, A.M., de Groot, K., Droste, H.J., 2002. Paleozoic stratigraphy and hydrocarbon habitat of the Arabian plate. AAPG Memoir 74, 483–515.

Kroner, U., Romer, R.L., 2013. Two plates — many subduction zones: the Variscan orogeny reconsidered. Gondwana Research 24, 298–329.

Landenberger, B., Collins, W.J., 1996. Derivation of A-type granites from a dehydrated charnockitic lower crust: evidence from the Chaelundi complex, eastern Australia. Journal of Petrology 37, 145–170.

Leake, E.B., Wooley, A.R., Arps, C.E.S., Birch, W.D., Gilbert, M.C., Grice, J.D., Hawthorne, F.C., Kato, A., Kisch, H.J., Krivovichev, V.G., Linthout, K., Laird, J., Mandarino, J., Maresch, W.V., Nickhel, E.H., Rock, N.M.S., Schumacher, J.C., Smith, D.C., Stephenson, N.C.N., Ungaretti, L., Whittaker, E.J.W., Youzhi, G., 1997. Nomenclature of amphiboles report of the subcommittee on amphiboles of the International Mineralogical Association Commission on New Minerals and Mineral Names. European Journal of Mineralogy 9, 623–651.

Li, Q.L., Li, X.H., Lan, Z.W., Guo, C.L., Yang, Y.N., Liu, Y., Tang, G.Q., 2013. Monazite and xenotime U–Th–Pb geochronology by ion microprobe: dating highly fractionated granites at Xihuashan tungsten mine, SE China. Contributions to Mineralogy and Petrology 166, 65–80.

Loucks, R.R., 1990. Discrimination of ophiolitic from nonophiolitic ultramafic–mafic allochthons in orogenic belts by the Al/Ti ratio in clinopyroxene. Geology 18, 346–349.

Meinhold, G., Reischmann, T., Kostopoulos, D., Lehnert, O., Matukov, D., Sergeev, S., 2008. Provenance of sediments during subduction of Palaeotethys: detrital zircon ages and olistolith analysis in Palaeozoic sediments from Chios Island, Greece. Palaeogeography, Palaeoclimatology, Palaeoecology 263, 71–91.

Moghadam, H.S., Ghorbani, G., Khedr, M.Z., Fazlnia, N., Chiaradia, M., Eyuboglu, Y., Santosh, M., Francisco, C.G., Martinez, M.L., Gourgaud, A., Arai, S., 2014a. Late Miocene K-rich volcanism in the Eslamieh Peninsula (Saray), NW Iran: Implications for geodynamic evolution of the Turkish–Iranian High Plateau. Gondwana Research 26, 1028–1050.

Moghadam, H.S., Li, X.-H., Ling, X.-X., Stern, R.J., Khedr, M.Z., Chiaradia, M., Ghorbani, G., Arai, S., Tamura, A., 2014b. Devonian to Permian evolution of the Paleo-Tethys

Ocean: new evidence from U–Pb zircon dating and Sr–Nd–Pb isotopes of the Darrehanjir–Mashhad "ophiolites", NE Iran. Gondwana Research http://dx.doi.org/10.1016/j.gr.2014.06.009.
Morimoto, M., Fabries, J., Ferguson, A.K., Ginzburg, I.V., Ross, M., Seifert, F.A., Zussman, J., Aoki, K., Gottardi, G., 1988. Nomenclature of pyroxenes. Mineralogical Magazine 52, 535–550.
Mushkin, A., Navon, O., Halicz, L., Hartmann, G., Stein, M., 2003. The petrogenesis of A-type magmas from the Amram Massif, southern Israel. Journal of Petrology 44, 815–832.
Namur, O., Charlier, B., Toplis, M.J., Higgins, M.D., Hounsell, V., Liegeois, J.P., Auwera, J.V., 2011. Differentiation of tholeiitic basalt to A-type granite in the Sept Iles layered intrusion, Canada. Journal of Petrology 52, 487–539.
Namur, O., Charlier, B., Holness, M.B., 2012. Dual origin of Fe–Ti–P gabbros by immiscibility and fractional crystallization of evolved tholeiitic basalts in the Sept Iles layered intrusion. Lithos 154, 100–114.
Okay, A.I., Demirbag, E., Kurt, H., Okay, N., Kuscu, I., 1999. An active, deep marine strike-slip basin along the North Anatolian fault in Turkey. Tectonics 18, 129–147.
Okay, A.I., Satir, M., Tuysuz, O., Akyuz, S., Chen, F., 2001. The tectonics of the Strandja Massif: late-Variscan and mid-Mesozoic deformation and metamorphism in the northern Aegean. International Journal of Earth Sciences 90, 217–233.
Okay, A.I., Bozkurt, E., Satir, M., Yigitbas, E., Crowley, Q.G., Shang, C.K., 2008. Defining the southern margin of Avalonia in the Pontides: geochronological data from the Late Proterozoic and Ordovician granitoids from NW Turkey. Tectonophysics 461, 252–264.
Patiño Douce, A.E., 1997. Generation of metaluminous A-type granites by low-pressure melting of calc-alkaline granitoids. Geology 25, 743–746.
Pearce, J.M., Peate, D.W., 1995. Tectonic implications of the composition of volcanic arc magmatism. Annual Review of Earth and Planetary Sciences 34, 251–285.
Pearce, J.A., Harris, N.B.W., Tindle, A.G., 1984. Trace-element discrimination diagrams for the tectonic interpretation of granitic-rocks. Journal of Petrology 25, 956–983.
Rolland, Y., Corsini, M., Demoux, A., 2009. Metamorphic and structural evolution of the Maures–Tanneron massif (SE Variscan chain): evidence of doming along a transpressional margin. Bulletin de la Societe Geologique de France 180, 217–230.
Rolland, Y., Sosson, M., Adamia, S., Sadradze, N., 2011. Prolonged Variscan to Alpine history of an active Eurasian margin (Georgia, Armenia) revealed by $^{40}Ar/^{39}Ar$ dating. Gondwana Research 20, 798–815.
Saccani, E., Azimzadeh, Z., Dilek, Y., Jahangiri, A., 2013. Geochronology and petrology of the Early Carboniferous Misho Mafic Complex (NW Iran), and implications for the melt evolution of Paleo-Tethyan rifting in Western Cimmeria. Lithos 162, 264–278.
Saccani, E., Allahyari, K., Rahimzadeh, B., 2014. Petrology and geochemistry of mafic magmatic rocks from the Sarve-Abad ophiolites (Kurdistan region, Iran): Evidence for interaction between MORB-type asthenosphere and OIB-type components in the southern Neo-Tethys Ocean. Tectonophysics 621, 132–147.
Shafaii Moghadam, H., Stern, R.J., 2014. Ophiolites of Iran: keys to understanding the tectonic evolution of SW Asia: (I) Paleozoic ophiolites. Journal of Asian Earth Sciences 91, 19–38.
Shafaii Moghadam, H., Khademi, M., Hu, Z., Stern, R.J., Santos, J.F., Wu, Y., 2015. Cadomian (Ediacaran -Cambrian) arc magmatism in the ChahJam -Biarjmand metamorphic complex (Iran): Magmatism along the northern active margin of Gondwana. Gondwana Research 27, 439–452.
Stampfli, G.M., Borel, G.D., 2002. A plate tectonic model for the Paleozoic and Mesozoic constrained by dynamic plate boundaries and restored synthetic oceanic isochrons. Earth and Planetary Science Letters 196, 17–33.
Stampfli, G.M., Mosar, J., Favre, P., Pillevuit, A., Vannay, J.C., 2001. Permo-Mesozoic evolution of the western Tethys realm: the Neo-Tethys East Mediterranean Basin connection. In: Ziegler, P., Cavazza, W., Robertson, A.H.F., Crasquin-Soleau, S. (Eds.), Peri-Tethys Memoir 5, Peri-Tethys Rift/Wrench Basins and Passive Margins vol. 186. Mémoires du Muséum National d'Histoire Naturelle, pp. 51–108.
Stern, R.J., Ren, M.H., Ali, K., Forster, H.J., Al Safarjalani, A., Nasir, S., Whitehouse, M.J., Leybourne, M.I., Romer, R.L., 2014. Early Carboniferous (similar to 357 Ma) crust beneath northern Arabia: tales from Tell Thannoun (southern Syria). Earth and Planetary Science Letters 393, 83–93.
Streckeisen, A., 1979. Classification and nomenclature of volcanic-rocks, lamprophyres, carbonatites, and melilitic rocks — recommendations and suggestions of the Iugs sub-commission on the systematics of igneous rocks. Geology 7, 331–335.
Tavakoli-Shirazi, S., de Lamotte, D.F., Wrobel-Daveau, J.C., Ringenbach, J.C., 2013. Pre-Permian uplift and diffuse extensional deformation in the High Zagros Belt (Iran): integration in the geodynamic evolution of the Arabian plate. Arabian Journal of Geosciences 6, 2329–2342.
Topuz, G., Altherr, R., Schwarz, W.H., Dokuz, A., Meyer, H.P., 2007. Variscan amphibolite-facies rocks from the Kurtoglu metamorphic complex (Gumushane area, Eastern Pontides, Turkey). International Journal of Earth Sciences 96, 861–873.
Topuz, G., Altherr, R., Siebel, W., Schwarz, W.H., Zack, T., Hasozbek, A., Barth, M., Satir, M., Sen, C., 2010. Carboniferous high-potassium I-type granitoid magmatism in the Eastern Pontides: the Gumushane pluton (NE Turkey). Lithos 116, 92–110.
Turner, S.P., Foden, J.D., Morrison, R.S., 1992. Derivation of some a-type magmas by fractionation of basaltic magma — an example from the Padthaway Ridge, South Australia. Lithos 28, 151–179.
von Raumer, J.F., Bussy, F., Stampfli, G.M., 2009. The Variscan evolution in the external massifs of the Alps and place in their Variscan framework. Comptes Rendus Geoscience 341, 239–252.
Whalen, J.B., Currie, K.L., Chappell, B.W., 1987. A-type granites — geochemical characteristics, discrimination and petrogenesis. Contributions to Mineralogy and Petrology 95, 407–419.
Yang, J.H., Wu, F.Y., Chung, S.L., Wilde, S.A., Chu, M.F., 2006. A hybrid origin for the Qianshan A-type granite, northeast China: geochemical and Sr–Nd–Hf isotopic evidence. Lithos 89, 89–106.
Zanchetta, S., Berra, F., Zanchi, A., Bergomi, M., Caridroit, M., Nicora, A., Heidarzadeh, G., 2013. The record of the Late Palaeozoic active margin of the Palaeotethys in NE Iran: constraints on the Cimmerian orogeny. Gondwana Research 24, 1237–1266.
Zanchi, A., Berra, F., Mattei, M., Ghassemi, M.R., Sabouri, J., 2006. Inversion tectonics in central Alborz, Iran. Journal of Structural Geology 28, 2023–2037.
Zhang, J., Ma, C., She, Z., 2012. An Early Cretaceous garnet-bearing metaluminous A-type granite intrusion in the East Qinling Orogen, central China: petrological, mineralogical and geochemical constraints. Geoscience Frontiers 3, 635–646.